Beyond: Undergraduate Research Journal

Volume 5 Article 1

Stress Intensity Factor - Simple Solution for a Complex Problem

Hamid A. Ghassri
Embry-Riddle Aeronautical University, ghassrih@my.erau.edu

Alberto Mello
melloa2@erau.edu

UNDERGRADUATE RESEARCH JOURNAL
Beyond

Stress Intensity Factor - Simple Solution for a Complex Problem

Hamid A. Ghassri & Alberto Mello

Abstract

This research explores the modeling of a cracked structure using a linear elastic finite element method (FEM) analysis with the objective of determining the stress intensity factor (SIF) for complex geometries. The analysis uses a mapping of the stress concentration area ahead of the crack tip to asymptotically determine the SIF. For model calibration, Irwin's approximation method was used in two known crack case solutions subjected to a uniform tensile loading (Mode I – Opening) with fixed geometric dimensions. With focus on aircraft airworthiness application, two more complex geometries with irregular stress distributions were analyzed and the results were extracted for future use in crack growth simulation.

Nomenclature

a	Length of crack
K_I , SIF	Stress Intensity factor for mode-I
LEFM	Linear Elastic Fracture mechanics
R	Distance away from crack tip
W	Width
ε	Strain
β, α	Geometric or correction factor
θ	Angle relative to cracked surface
E	Modulus of Elasticity
σ_{ref}	Nominal or reference stress
σ_x	Local stress in the x-axis
σ_y	Local stress in the y-axis
$\sigma_{x,y}$	Bidirectional local stress

Background

The study of cracked structures and fracture mechanics is a subject of great importance within the aerospace engineering community. Airframe structures are always under the constant threat of failure from fatigue. Once a potential failure is detected, such as a crack, corrective action must be prescribed to ensure that the structure is safe for continuous service (Broek, 1989). At this point, it is important to outline relevant information such as basic theory of LEFM and related engineering programs used in the application of damage tolerance analysis.

A study performed by Findlay and Harrison (2002) showed that of all aircraft related accidents due to defects and structural failures, 55% are fatigue related. If combined with other failure modes such as corrosion, the percentage increases to 71%. This makes fatigue and crack propagation an important subject for further research, mainly considering the complex nature of crack growth in engineering materials (Kanninen & Popelar, 1985). It is found that materials can fail before their ultimate strength when in presence of crack (Dowling, 2012). This effect is very dependent of a material property defined as fracture toughness. The effect of crack on structures can be analyzed using linear elasticity theory, which predicts that stress at ahead of a crack in a linear elastic medium tends to approach infinity at the crack tip, as long as the singularity at the crack tip is isolated (Broek, 1989). The magnitude of stress in the vicinity of crack tip can be linked with the distance to the crack tip and geometric parameters, and used for determining the stress intensity factor, SIF (Broek, 1989). SIF is defined as the driver parameter characterizing the state of stress near a crack tip on linear elastic fracture mechanics, in a region defined as the K-dominant zone. In this region, the SIF can be related with the remote loading stress (Broek, 1989). In the present study, the loading condition was focused on Mode I-opening, which can be represented as tensile stress normal to the crack as shown in Fig.1.

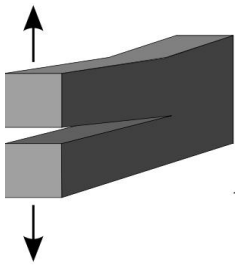

Figure 1: Mode I: Opening

The SIF of a Mode-I opening crack loading is dependent on the geometric parameters and crack size of the component. When considering a specimen and crack of arbitrary shape and size, the x and y stress values ahead of the crack tip can be determined using Eqn.1 (Broek, 1989). For θ = 0 the Eqn.1 simplifies to Eqn.2.

$$\sigma_{x,y} = \frac{K_1}{\sqrt{2\pi r}} \cos\frac{\theta}{2}\left(1 - \sin\frac{\theta}{2} - \sin\frac{3\theta}{2}\right) \quad (1)$$

$$\sigma_{x,y} = \frac{K_1}{\sqrt{2\pi r}} \quad (2)$$

This is further illustrated in Fig. 2, where there is a crack present in some arbitrary body in Mode-I loading condition. In ductile materials, a region of plasticity is formed ahead of the crack tip which is known as the process or plastic zone (Dowling, 2012). The higher the applied stress, the larger is the plastic zone, which also depends on the yield stress of the material (Dowling, 2012). If a plastic zone were not formed, then as the distance to crack tip, r, approaches to zero, the stress would go to infinity. This forms what is known as a "singularity state of stress", which has an order of magnitude of $1/\sqrt{r}$ along the x-axis of reference. A solution considering a linear elastic analysis is valid near a crack tip, but not inside the plastic zone, where the real stress is limited to a local yielding condition (Broek, 1989).

A general equation for the SIF as a function of the crack size and the remote applied stress is also proposed in the literature defined by Eqn. 3.

$$K_1 = \beta\sigma_{ref}\sqrt{\pi a} \quad (3)$$

A correction factor, β, is applied to the general SIF equation initially proposed by Westergaard (1939). Westergaard's solution is for a center crack in an

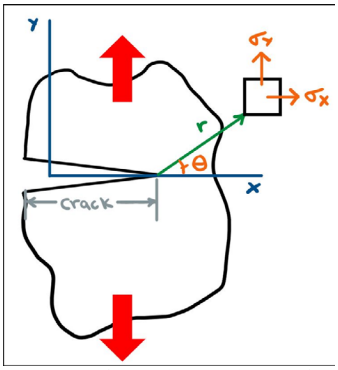

Figure 2: Stress away from the crack tip of an arbitrary body under mode-I tensile loading.

infinite plate. The correction factor, β, is included to account for asymmetry and the finite geometric dimensions of a specimen. To determine the correction factor, we may apply direct and indirect use of handbook solutions, or a combination of the two. Indirect use of handbook solutions can be solved for using superposition and compounding methods. Empirical handbook solutions for simple crack models can be simply added as exemplified in Fig.3 (Broek, 1989).

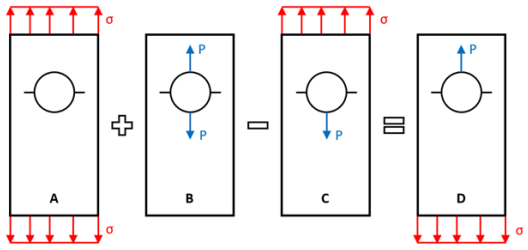

Figure 3: Determining Stress intensity factor by superposition, $K^A + K^B - K^C = K^D$ (Broek, 1989).

Another method that can be used involves finite element analysis (FEA) of a modeled crack. Correction factor is normally a function of loading condition, crack size, and specimen dimensions. For instance, for an arbitrary crack size in Mode-I, β = β(a/w), where w in this case is the width of the cracked component (Perez, 2018).

There are solutions in the literature for common geometries and loading conditions. One important aspect of Eqn. 3, it is that a given β is linked with a defined remote stress, normally referred as reference stress. In the instance of simple structure with uniform remote stress, there is no difficulty linking this stress with the proposed correction factor solution Eqn. 3. In the case where the stress distribution is non-uniform and the component geometry is complex,

it may not be as obvious which stress should be used in the expression for stress intensity factor, or how to compose the SIF solution. It is important that any proposed SIF solution must also make clear what is the reference stress being considered in Eqn. 3.

The mathematical definition of SIF based on local stress is given by Eqn. 4. Therefore, if local stress can be mapped around the crack tip, Eqn. 4 can be used to estimate the SIF for any geometry.

$$K_1 = \lim_{r \to 0} \sigma_y \sqrt{2\pi r} \tag{4}$$

The process considers using Eqn. 4 to asymptotically obtain the SIF from the mapped stress ahead of crack tip, out of the plastic zone, and consequently to determine the correction factor for a given reference stress and crack size by comparing the SIF results with Eqn. 3. It is important to note that Eqn.4 is valid in a region defined as K-dominant zone, which does not include the plastic zone, and it is free of boundary effects (Broek, 1989). The result for $r \to 0$ is obtained by curve extrapolation, what forces a singularity of $1/\sqrt{r}$ for the local stress.

FEMAP, an engineering analysis program with pre- and post-processing capabilities which can compute complex finite element models, can be used to model cracks of various sizes on several types of plates. This program provides the ability to import computer-aided drafting (CAD) models and has several meshing tools to help creating a finite element model and solving problems isolating the singularity caused by a crack. FEMAP has post-processing functionality which allows users to interpret analysis results in various solvers such as MSC NASTRAN. This solver is widely used in the aerospace industry and is also recognized by Federal Aviation Administration (FAA) as an acceptable standard for airframe design certification. MSC NASTRAN, combined with the pre-processing abilities of FEMAP to validate boundary and load conditions to evaluate different designs and material configuration, has proven to be a very robust FEA tool.

Methods

To determine the SIF's, finite element models containing cracks were created using FEMAP. There was a need to first assess which stress should be analyzed in the testing of the various plates: Von Mises stress yield criterion or max principle stress criterion. Von Mises stress yield criterion is based on the yielding capabilities of a ductile material under a complex loading condition. This is a scalar value which is derived from the existing stresses within the studied specimen (Broek, 1989). Maximum principal stresses are the maximum values of the normal stresses which exist when a structure is experiencing a multiaxial stress state (Dowling, 2012). This is normally used in the analysis of brittle materials under complex loading conditions. For the purpose of studying cracked components, it would be best to examine the component considering maximum principle stress since it is well known that a crack propagates perpendicularly to the major principal stress in Mode-I, despite the plastic zone size be better defined using von Mises stress.

An initial study was required to determine whether a linear or non-linear static analysis was needed for the simulations. A linear static analysis is conducted when there is a linear relation between the applied forces and displacements, which is valid for structural problems where the stresses remain in the linear elastic region of a stress vs strain curve, as shown in Fig. 4.

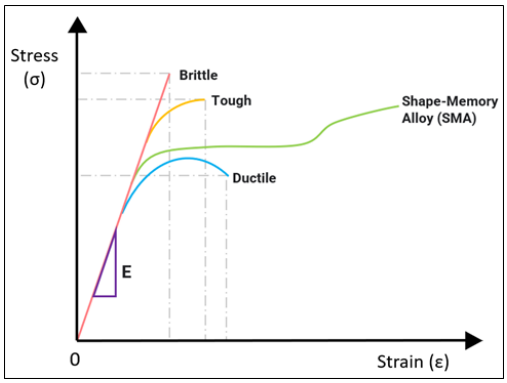

Figure 4: Stress vs Stain curve of various material types. (Perez, 2018)

It can be noted that the majority of aerospace materials can be classified as linear elastic- plastic, for which there exist two states which are separated by certain stress level called the yielding point or yield stress. Under some arbitrary tensile loading condition, a material will elongate or strain as the stress increases. The region before a material yields is called the linear elastic region, as mentioned before. This means that the material, when unloaded, will

retain its original shape and there will not be any permanent deformation to the structure (Perez, 2018). If the stress exceeds the yielding stress of the material, it will begin to enter a nonlinear region or the region of plasticity, where there will be permanent deformation to the structure. As long as the net stress in the material cross section containing the crack plane remains in the elastic region, and the yielding is limited to a small plastic zone near the crack tip, the SIF will be representative and the correction factor will not depend on the level of stress. This means that despite a plastic zone formed at the crack tip, the remaining of the component is in the elastic regime. With this, there was no need to change the static analysis to find nonlinear solutions since the remote tensile stress was kept low and the analysis could be fully linear. The analysis is valid for any type of material, since the solution is always obtained out of the plastic zone, as discussed previously.

However, to illustrate the methodology and to obtain the stress map via FEA, a commercially available aircraft structural material was chosen. The material is ductile and used in aircraft primary structures, such as the fuselage and wings. Aluminum alloy 6061 is precipitation-hardened and contains a alloying mixture of magnesium and silicon. It is also corrosion resistant, and it is found to be easily workable when extruded or welded. Material properties (Metals Handbook Vol.2, 1990), along with the proposed specimen's geometry and loading, for the analyzed components can be found in Table.1.

Table 1: Tabulated values specimen material, structural dimensions, and reference load.

Aluminum Alloy 6061-T651[a]					
Density (g/cc)	Tensile Strength (MPa)	Modulus of Elasticity (GPa)	Shear Strength (MPa)	Shear Modulus (GPa)	Poissons Ratio
2.7	276	68.9	207	26	0.33
Through Crack at Edge of Plate					
Plate Width (mm)	Plate Height (mm)	Plate Thickness (mm)	Reference Load (N)	Reference Stress (MPa)	
100	200	6.35	97350	153.3	
Through Crack from Hole in A Plate					
Plate Width (mm)	Plate Height (mm)	Plate Thickness (mm)	Hole Diameter (mm)	Reference Load (N)	Reference Stress (MPa)
100	200	6.35	20	97350	153.3
Through Crack at Slot in A Plate					
Plate Width (mm)	Plate Height (mm)	Plate Thickness (mm)	Slot Diameter (mm)	Reference Load (N)	Reference Stress (MPa)
100	200	6.35	40	97350	153.3
Through Crack in A Complex Plate					
Plate Width (mm)	Plate Height (mm)	Plate Thickness (mm)	Reference Load (N)	Reference Stress (MPa)	
200	100	6.35	97350	153.3	

Note: [a](Metals Handbook Vol, 2 1990).

As an experimental control, the structural dimensions of 100 mm x 200 mm x 6.35 mm was used to all the plate components. The independent variable for each simulation is the initial crack size, and the dependent variables are the SIF's and the geometric correction factors.

It was critical to determine the loads and boundary conditions of the model for analysis. The loads applied to a specimen are defined as either the mechanical forces or thermal loadings which act on the body. The boundary condition set on a specimen is defined as the environmental factors which directly influence the behavior of the external and internal loads which act on the component. An example of a boundary condition can be a constraint such as a pin, roller or a fixed point which prevent rotations or displacements from occurring when a force is introduced to the system. Fig.5 shows what boundary conditions were placed on the plate components for the simulations. The red arrows represent a uniform tensile load acting on the top of the plates. The tensile load used in the

simulations remained constant. The green triangles represent a uniform fixed constraint which prevent axial displacements and rotation at the bottom of the plates. A real example of this experiment model would be a plate being pulled on by a tensile test bench, where a portion of the top and bottom of the plate would be fixed with a vise grip mechanism with only the top being able to have vertical displacement. The specimens are designed long enough to make sure the stress was completely homogenized in the region of the crack.

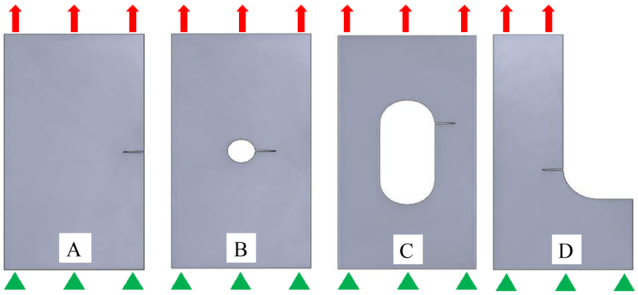

Figure 5: Specimen used for simulation with a through crack initiated.

The final design criteria addressed was the mesh refinement. Since the mesh size of a model directly influences the accuracy and speed of the simulation, mesh sizing is crucial for the correct solution of a FEM problem. It is commonly known that the smaller the elements, the more accurate the results are. However, processing time, memory and hardware capability may impose limitations to mesh refinement.

The model for these experiments was determined to be a 2D plate with cracks which were geometrically formed from an ellipse shape, as shown in Fig. 6. The mesh was then simplified to tangential quad element shapes. It was found that quad element types are preferred over tria element types because of stress distribution representation. In tria element types, the stress distribution is constant, while quad element stress is linearly interpolated between nodes, which means that results are modeled with higher precision using the same number elements (Goelke, 2014). An advantage to using tria element types is the capability for results to be processed faster, and tria shape can form to most complex geometric structures without the need of pre-processing the mesh grids.

Examples of the mesh grids used in the simulations are shown in Fig. 6 and Fig. 7. It was key for the elements to remain as uniform as possible to prevent any abnormalities in the final calculation. It should be noted that the arrangement of the elements around curvatures still retain a quad element shape without the need of creating tria elements to compensate for complex geometric structure. The models contained a mesh with 2D planer elements, which had an element size of 0.5 mm x 0.5 mm. Even though the ellipse format was used in the crack tip, the singularity $1/\sqrt{r}$ was enforced in the solution by obtaining the SIF at the crack tip via extrapolation using Eqn. 4.

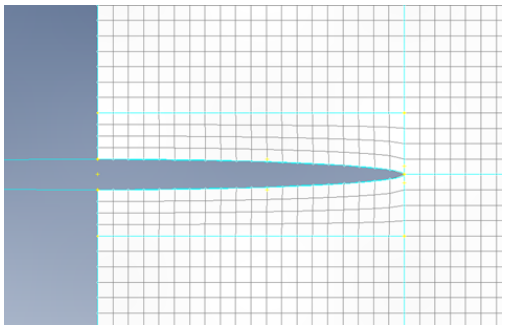

Figure 6: Mapped mesh region for through crack at the edge of a plate.

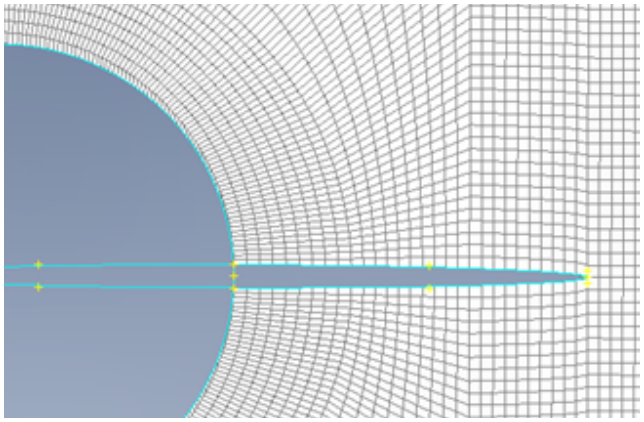

Figure 7: Mapped mesh region for through crack from a hole in a plate.

For the post-processing of the results from the FEA, a method for mapping the stress ahead of crack tip was needed to be devised. It was observed that selecting individual elements along the centerline of the crack tip was ideal for determining the SIF derived from the maximum principle stresses. These stress values are then plotted and compared. For instance, in Fig. 6 the blue line running vertically from the crack tip would limit the area of study. From this mapped region, SIF can be determined

as explained before. This process is known as Irwin's approximation (Irwin, 1957). The results then produce a plot for SIF, as shown in Fig. 8. A trendline is created in the SIF plot to find the y-intercept at the crack tip or at r = 0. This is the SIF value which will be used in determining the correction factor for a given crack length. This would represent the SIF defined in Eqn. 4, in the limit as $r \rightarrow 0$. The geometric factor values for the simple structures would then be compared to that of the literature and plotted with percent error values within 10%.

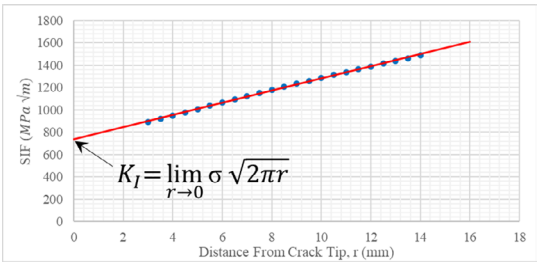

Figure 8: Asymptotic solution for stress intensity factor determined from mapped stress away from the crack tip.

As proof of concept, the same procedure was applied to a more complex geometry with a crack emerging from a hole (Fig. 5-B) for reproducibility check. Once the FEM sensitivity analysis was completed and the result matched the expected SIF for the previously known solutions, the model was considered calibrated. The model was then applied to even more complex geometries that could represent structure cutouts and stress concentrations in aerospace structures, depicted in Fig. 5 C-D.

Results

Fig. 9 shows the FEM mapping for a crack in the edge (EC) of a plate (Fig. 5-A), for which the SIF solutions are well known and explored in the literature. The figure shows the stress fields for crack sizes of 5 mm and 10 mm. The same process was repeated for 15 mm and 20 mm crack sizes.

The stress mapping along the horizontal line ahead of the crack tip is summarized in Fig. 10, for the analyzed crack sizes.

The values for local stress were then inserted into Eqn. 4, and the LEFM value for SIF was estimated as an asymptotic value forcing a stress singularity proportional to $1/\sqrt{r}$ at the crack tip, as exemplified in Fig. 8. The results for crack sizes of 5-, 10-, 15- and 20-mm are depicted in Fig. 11.

The results obtained from Fig. 11 were then plugged into Eqn. 3, and the correction factors, β's, for the current crack case were plotted against crack size and compared with the values in the literature (Mello, 1998, 2005). The results obtained from a crack growth software are expected to have an accuracy within 10%. The uncertainty for the model is represented by the error bars in Fig. 12.

The results for the correction factors shown in Fig. 12 are tabulated for best comparison with the expected values. It can be seen from Table 2 that all results are within the expected accuracy for the model (error < 10%).

As we have described in the previous section, the procedure was repeated for a more complex geometry, but still with solution available in the literature for comparison. As a repeatability check, we have applied the FEM approach to a crack emerging from a hole (CH). An FEM illustration (for CH = 5 mm) is shown in Fig. 13, and the processed results are shown in Fig. 14, Fig. 15 and Fig. 16. Table 1 shows the final values for the correction factors with the measured errors. Here again the error is within the acceptable values (error < 10%).

As example of practical applications, we have used the proposed procedure to determine the correction factors as function of crack size for the two types of geometries proposed in Fig. 5 C-D. Those geometries can be modeled to represent a cutout slot (CS) in aircraft longerons or bulkheads (Fig. 5-C), and complex crack case (CX) in structure corners (Fig. 5-D), which are typically present in aircraft structures. Those types of geometries, even being common in airframes, are not easily modeled, and each case will involve complex analysis to determine the SIF correction factors.

Fig. 17 and Fig. 21 show examples of the stress fields obtained with FEA for crack emerging from a slot and from a stress concentration corner, respectively, as depicted in Fig. 5 C-D. Fig. 18 and Fig. 22 plot the stress values ahead of the crack tip for both cases, and Fig. 19 and Fig. 23 show the SIF values obtained via asymptotic solutions. Finally, Fig. 20 and Fig. 24 show the charts of the correction factors as function of crack length for the

two complex geometries exemplified in Fig. 5 C-D.

Discussion

Once the stress field maps are obtained with finite element analysis, The SIF's were determined by graphically extrapolating Eqn. 4. The results for the correction factors were then calculated using Eqn. 3. It was shown that the results obtained for the two known cases proved the method has good accuracy, being within 10% of error, when compared with standard solutions available in the literature. Certainty within 10% is the normal claimed accuracy for the available SIF solutions.

Once the methodology was defined, the process could be applied for more complex geometries. For what the application of the method is concerned, the level of difficulty for complex geometries is the same as for simple geometries. The limitation of the structure complexity will be defined by the ability to model the component and perform the finite element analysis, which has become virtually boundless considering all the modeling tools commercially available for applied engineering and research studies.

For the study of the complex plate, it was critical to understand which cross-sectional area was to be defined for the reference stress. As shown in Fig 5-D, the reference stress in this case was decided to be the remote stress acting in the larger portion of the plate (bottom). So, the solution presented in Fig. 24 must be used computing the acting stress based on the larger transverse area of the plate.

Conclusion

The use of an engineering software which performs linear static analysis calculations such as FEMAP showed good potential in the application of crack modeling, stress mapping, and SIF determination. Complex geometries are present in real aerospace structures, and the SIF solutions are rarely available for prompt application. This methodology defines a simple procedure to find SIF solutions for any geometry and it is applicable to any material. The geometries shown in Fig. 5 C-D were selected as example because the lack of analytical solution and their common use within aerospace structures. This study is especially helpful in the application of damage tolerance analysis to comply with aircraft airworthiness. This work can be furthered studied by researching other methods of retrieving the SIF of a cracked components, such as using energy equations to be compared to that of Irwin's approximation method. Another suggestion to improve the current study is the analysis of part-thru cracks, such as surface cracks and corner cracks of geometric structures.

References

American Society for Metals, & Benjamin, D. (1990). Properties and Selection: Nonferrous Alloys and Pure Metals (Metals Handbook) (10th ed.). American Society for Metals.

Broek, D. (1989). The Practical Use of Fracture Mechanics (Softcover reprint of the original 1st ed. 1989 ed.). Springer.

Dowling, N. E. (2009). Mechanical Behavior of Materials: Engineering Methods for Deformation, Fracture, and Fatigue. Pearson Prentice Hall.

Findlay, S., & Harrison, N. (2002). Why aircraft fail. Materials Today, 5(11), 18–25. https://doi.org/10.1016/s1369-7021(02)01138-0

Gokhale, N. S. (2008). Practical Finite Element Analysis (1st ed.). Finite To Infinite.

Irwin, G. R. (1957). Analysis of Stresses and Strains Near the End of a Crack Traversing a Plate. Journal of Applied Mechanics, 24(3), 361–364. https://doi.org/10.1115/1.4011547

Kundu, T. (2008). Fundamentals of Fracture Mechanics (1st ed.). CRC Press.

Mello, A. W. (1998). CRACK 2000 Program User's Manual (2.1 ed.). Campo Montenegro.

Mello, A. W. (2005). CRACK 2000 (3.0) [Engineering Software for Damage Tolerance Analysis and Fatigue]. Campo Montenegro.

Perez, N. (2018). Fracture Mechanics (Softcover reprint of the original 2nd ed. 2017 ed.). Springer.

Popelar, C. H., & Kanninen, M. F. (1985). Advanced Fracture Mechanics (Oxford Engineering Science Series, 15) (1st ed.). Oxford University Press.

Westergaard, H. M. (1939). Bearing Pressures and Cracks: Bearing Pressures Through a Slightly Waved Surface or Through a Nearly Flat Part of a Cylinder, and Related Problems of Cracks. Journal of Applied Mechanics, 6(2), A49–A53. https://doi.org/10.1115/1.4008919

Appendix 1 Figures

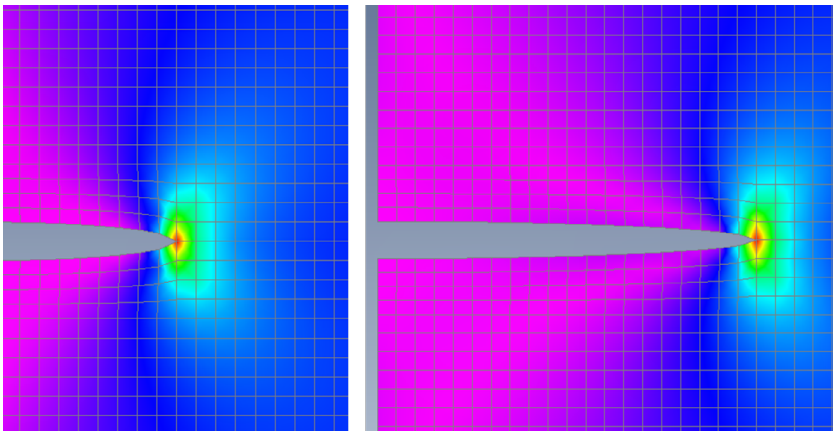

Figure 9: Mapped stress field away from the crack tip for a plate in Fig.5A. (5-mm crack [left], 10-mm crack [right]).

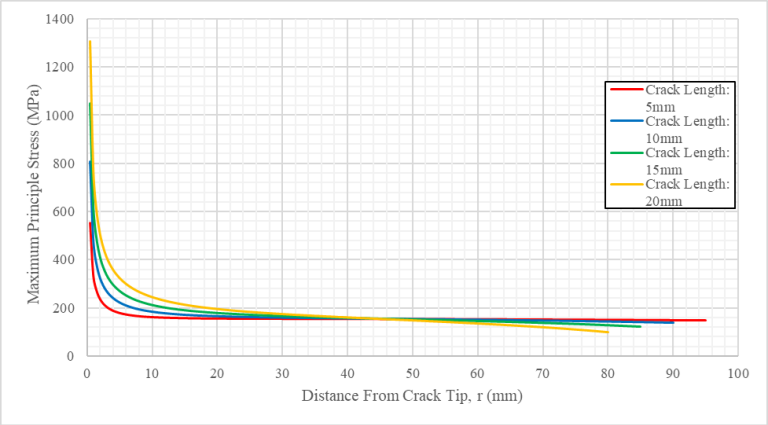

Figure 10: Maximum principle stress away from crack tip for various through crack sizes at edge (EC) of plate.

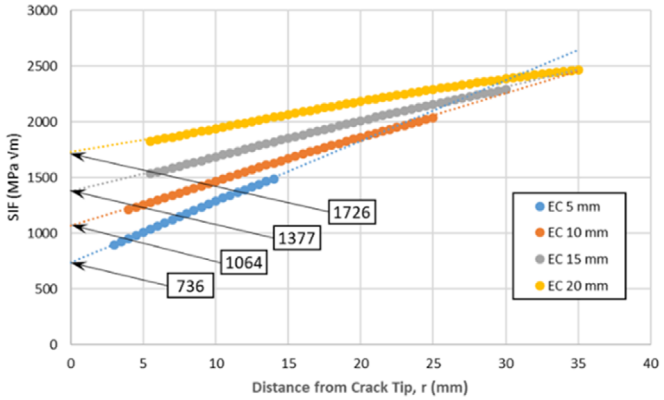

Figure 11: Asymptotic solution for the stress intensity factor for through edge crack (EC) in a plate (Fig.5A), for 5-, 10-, 15- and 20-mm cracks.

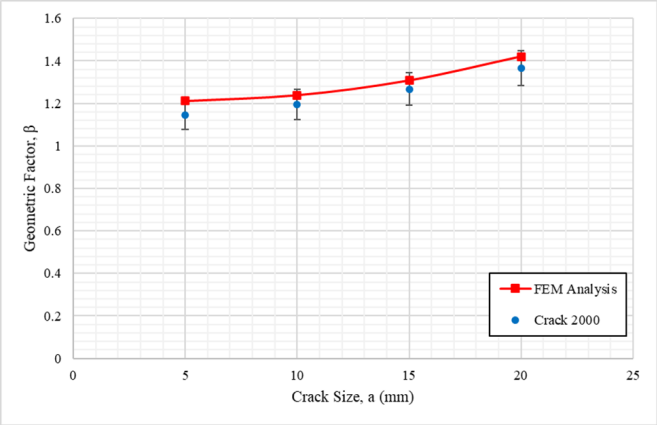

Figure 12: Geometric Factor for various crack sizes for the crack at edge of plate model. Results from current work and from literature (Crack 2000, 1998, 2005).

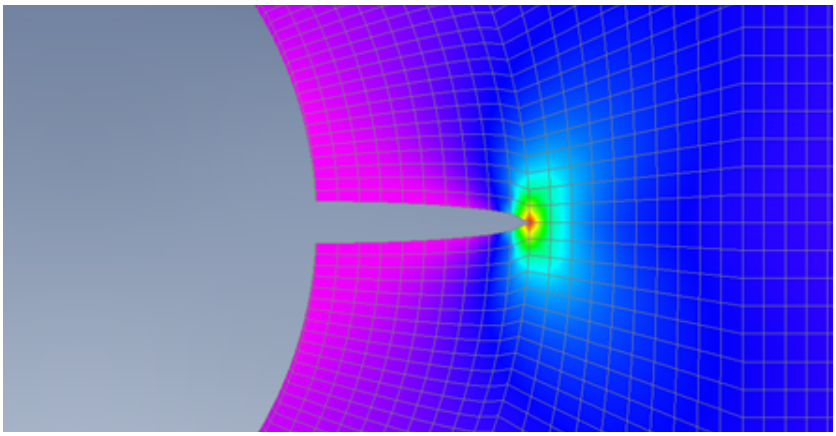

Figure 13: Mapped stress field away from the crack tip for a 5-mm crack in a hole (Model in Fig.5B).

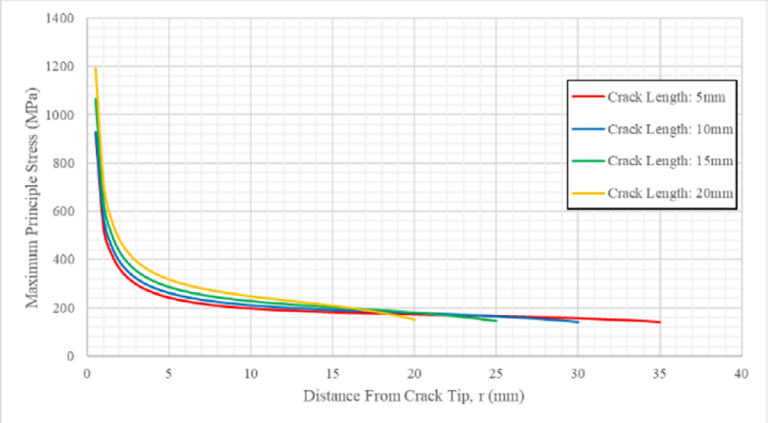

Figure 14: Maximum principle stress away from crack tip for various through crack from hole in a plate.

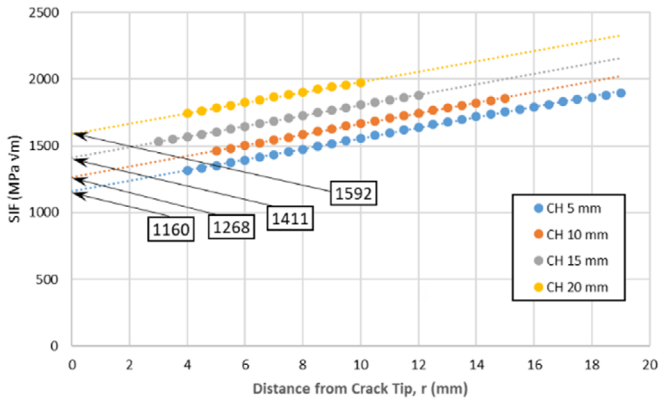

Figure 15: Asymptotic solution for the stress intensity factor for through crack from hole (CH) in a plate (Fig.5B), for 5-, 10-, 15- and 20-mm cracks.

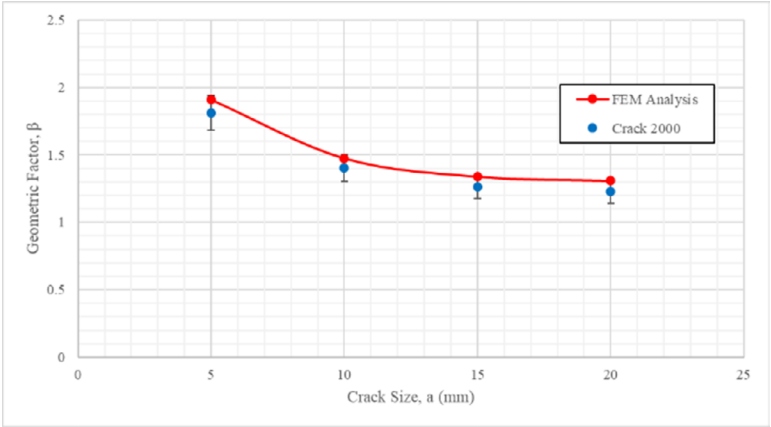

Figure 16: Geometric Factor for various through cracks from hole in a plate.

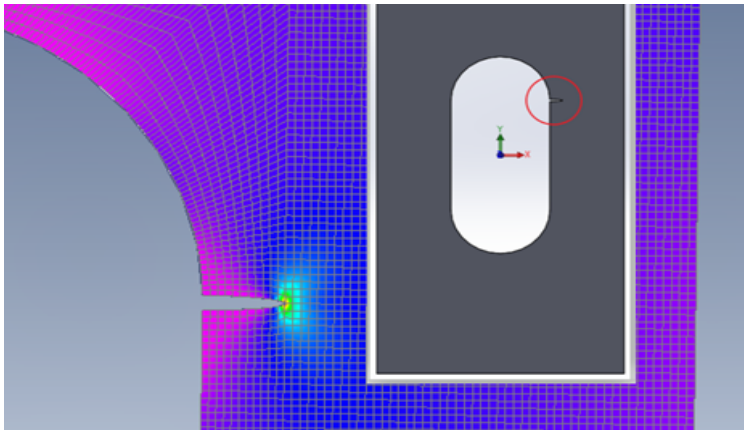

Figure 17: Mapped stress field away from the crack tip for 5-mm crack from slot in a plate (Model in Fig.5C).

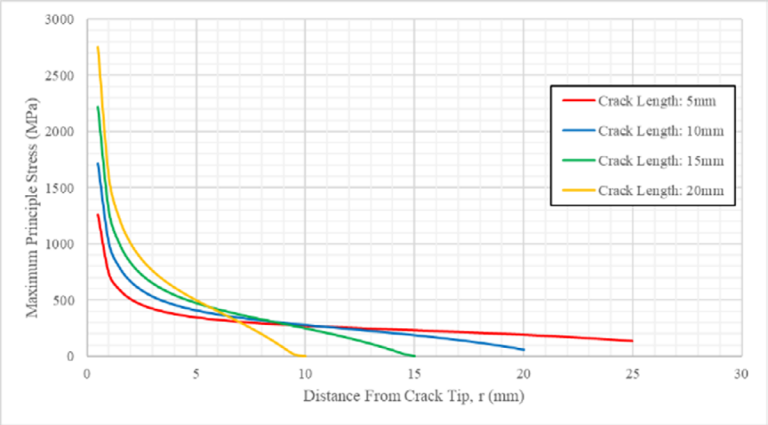

Figure 18: Maximum principle stress away from crack tip for various through crack from slot (CS) in a plate.

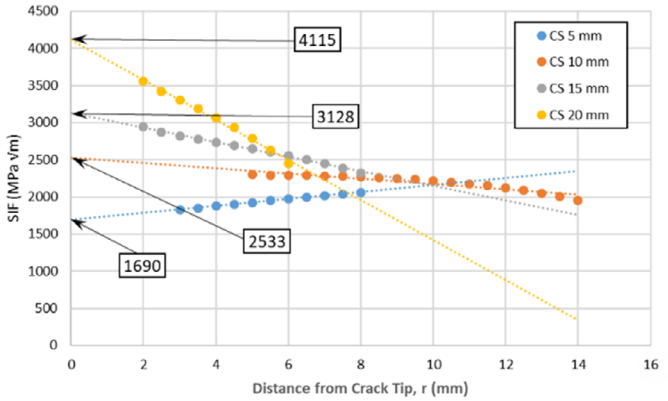

Figure 19: Asymptotic solution for the stress intensity factor for through crack from slot in a plate (CS) in a plate (Fig.5C), for 5-, 10-, 15- and 20-mm cracks.

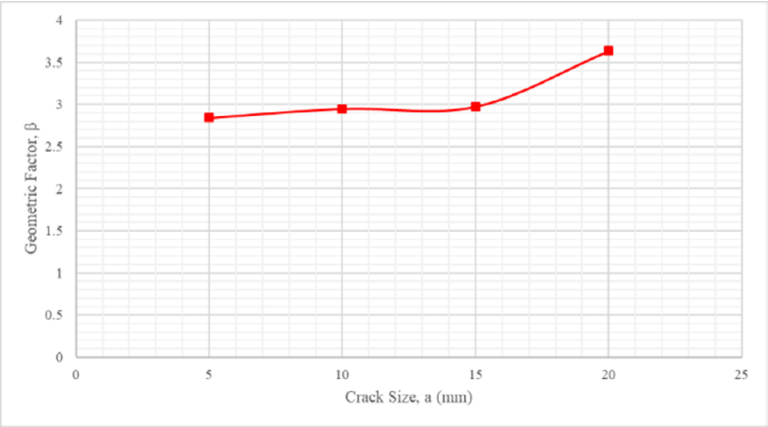

Figure 20: Geometric Factor for various through cracks from slot (CS) in a plate.

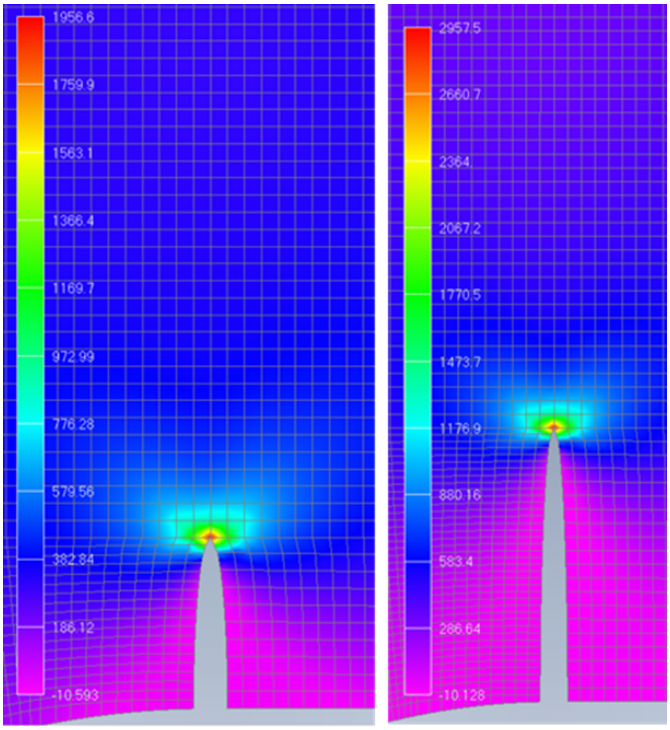

Figure 21: Mapped stress field away from the crack tip for 5-mm (left) and 10-mm (right) cracks from slot in a plate (Model in Fig.5D).

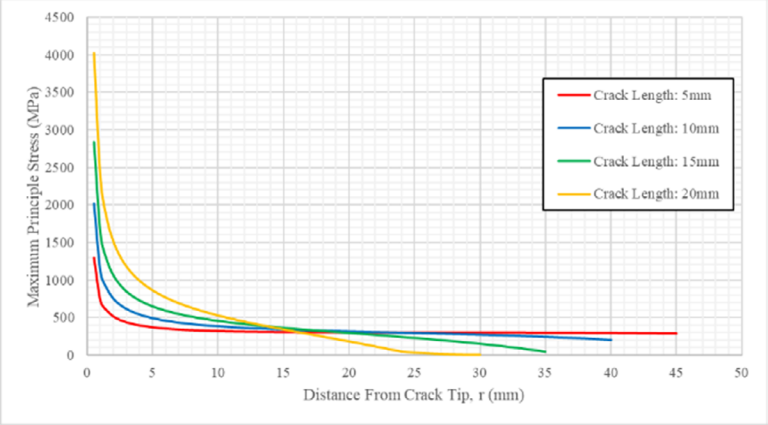

Figure 22: Maximum principle stress way from crack tip for various through crack from a complex plate.

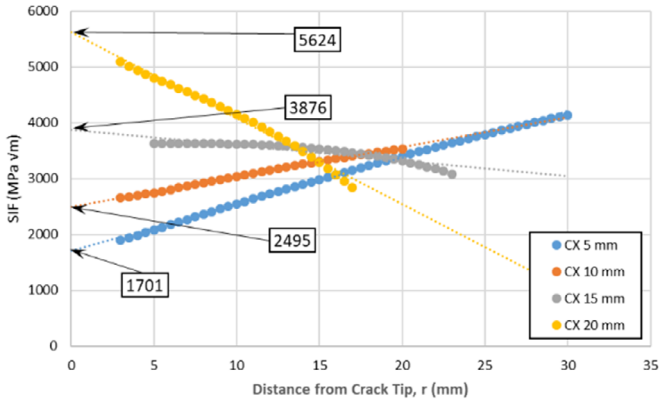

Figure 23: Asymptotic solution for the stress intensity factor for through crack on a complex (CX) plate (Fig.5D), for 5-, 10-, 15- and 20-mm cracks.

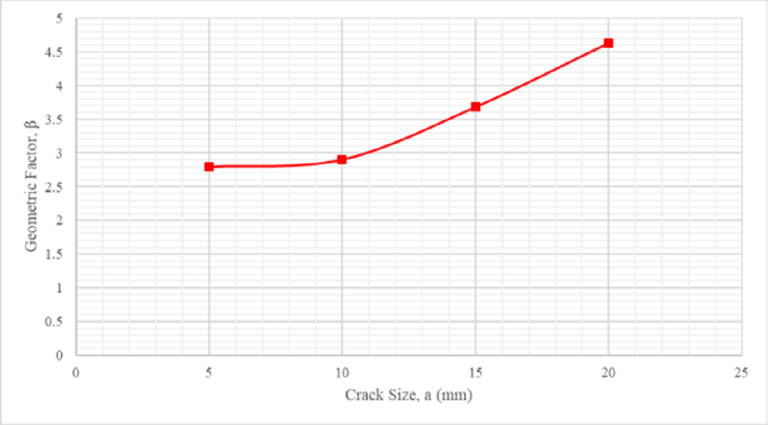

Figure 24: Geometric Factor for various through cracks from a complex plate.

Appendix 2 Tables

Table 2: Tabulated values for SIF and geometric factor for various through cracks at edge of plate.

Through Crack at Edge of Plate				
CRACK SIZE (mm)	SIF ($MP\alpha\sqrt{m}$)	Geometric Factor (FEM Analysis)	Geometric Factor (Literature)	Geometric Factor Percent Error (%)
5	736	1.211	1.147	5.626
10	1064	1.239	1.196	3.604
15	1377	1.308	1.263	3.171
20	1726	1.420	1.367	3.894

Table 3: Tabulated values for SIF and for geometric factor for various through cracks from hole in plate.

Through Crack from Hole in a Plate				
CRACK SIZE (mm)	SIF ($MP\alpha\sqrt{m}$)	Geometric Factor (FEM Analysis)	Geometric Factor (Literature)	Geometric Factor Percent Error (%)
5	1160	1.909	1.812	5.365
10	1268	1.476	1.405	5.049
15	1411	1.340	1.263	6.137
20	1592	1.309	1.227	6.740